# Spin waves and phonons in $La_{1-x}Sr_xMnO_3$ ($x=0.09$, 0.125): Dynamical signatures of low-temperature phase transitions for $x=0.125$

F. Moussa,[1] M. Hennion,[1] F. Wang,[1] P. Kober,[1] J. Rodríguez-Carvajal,[1] P. Reutler,[2,3] L. Pinsard,[2] and A. Revcolevschi[2]
[1]*Laboratoire Léon Brillouin, CEA-CNRS, CEA Saclay, F-91191 Gif-sur-Yvette Cedex, France*
[2]*Laboratoire de Physico-Chimie des Solides, Université Paris-Sud, F-91405 Orsay Cedex, France*
[3]*RWTH, II. Physik Institut, Aachen, D-52056, Germany*
(Received 23 September 2002; revised manuscript received 10 February 2003; published 20 June 2003)

Neutron scattering has been used to study static and dynamic magnetic properties of $La_{1-x}Sr_xMnO_3$ with $x=0.09$ and 0.125. The $x=0.09$ compound appears as a limit case of an inhomogeneous canted antiferromagnetic (CAF) *A*-type structure. Related to the mean AF medium, anisotropic superexchange integrals are determined from the measurement of a high energy spin wave branch. Coexisting with this mean state, ferromagnetic (F) hole-rich platelets spread in the basal F plane, close to the limit of percolation. Related to these F inhomogeneities, an anisotropic magnetic coupling is determined from an anisotropic low energy spin wave branch. The $x=0.125$ compound exhibits, below $T_C$, a ferromagnetic and metallic phase (FM). At $T_{O'O''}$, a magnetostructural transition occurs leading to a F and insulating phase (FI) with unusual properties: in the whole q range, a splitting of the spin wave spectrum is observed. A large gap opens at (0,0,0.5). At this point and beyond, the energy of the spin waves locks on the phonon energy values. The temperature evolution of the splitted magnetic modes and of the phonons is presented, with marked signatures of both transitions. These results are discussed in the frame of existing theories.

DOI: 10.1103/PhysRevB.67.214430 PACS number(s): 75.30.Ds, 75.30.Et, 75.30.Kz, 75.30.Mb

## I. INTRODUCTION

The properties of the ferromagnetic and metallic (FM) phase of the manganite compounds, with colossal magnetoresistance effects (CMR), are very unusual. They are deeply distinct from the properties of transition metals. In the ferromagnetic metallic systems, the spin wave stiffness constant increases with the Curie temperature $T_C$ and with the numbers of charge carriers. In the CMR FM phase of the $La_{1-x}Sr_xMnO_3$ manganites, whatever $T_c$ and the amount of doping *x*, the spin wave stiffness constant has more or less the same value.[1] Moreover, for the compounds with the lowest values of $T_c$, a strong renormalization of magnons near the zone boundary is observed. This softening appears together with an increase of the damping, characteristic of magnon-phonon coupling, and with a locking on a neighboring optical phonon branch, at low temperature.[2] A mere theory of double exchange[3,4] cannot explain these characteristics. An advanced explanation is the scattering of magnons by the orbital and charge fluctuations and by the Jahn-Teller (JT) phonon.[5] The effect of an orbital liquid order on the spin wave stiffness constant, has been also considered.[6]

Furthermore, in the low doped systems, the delicately balanced interplay among charge, lattice, orbital, and spin degrees of freedom produces amazing properties. When long-range Coulomb interactions are considered, a microscopically charged inhomogeneous state is predicted. Among numerous theoretical works on those topics, see Refs. 7–10. These models can explain the inhomogeneous canted antiferromagnetic (CAF) state found in the manganite phase diagram in the low doping rate range. But the occurrence of a ferromagnetic and insulating (FI) state in the phase diagram, just between the CAF state ($0<x<0.1$) and the FM CMR state ($x\geqslant 0.17$), has not been predicted neither by the double exchange (DE) model nor by any other. To better understand these properties, it is of special interest to study the behavior of the spin waves in manganite compounds which exhibit such a FI phase. We present here a summary of a detailed study of the spin waves and of the low energy phonon branches, and their temperature behavior, in two compounds with two limit doping rate values. The comparison betweeen both samples is very instructive. We shall show that, in the $x_{Sr}=0.09$ compound, the magnetic couplings are essentially of two kinds, the first one, of mainly superexchange (SE) origin, associated with the mean AF matrix, and the second one, rather of double exchange (DE) nature, associated with the ferromagnetic inhomogeneities, close to the limit of percolation. This confirms the inhomogeneous character already found in other low-doped Ca and Sr manganites.[11–15] The TA, LA, LO phonons measured in this compound do not show any anomalies at the magnetic transitions.

$La_{0.875}Sr_{0.125}MnO_3$, which is a limit case before the CMR FM phase, displays, below the (JT) transition temperature $T_{JT}=280$ K, first a transition towards a ferromagnetic and metallic (FM) state, at $T_C=181$ K, without any CMR effect, then, a magneto-structural transition into a ferromagnetic and insulating (FI) state, at $T_{O'O''}=159$ K, with peculiar properties. This FI phase is characterized by a jump in the magnetization and by the occurrence of superstructure peaks.[16–18] This study, by means of neutron scattering, reveals, at the same time, lattice and magnetic dynamical signatures of both low temperature transitions, $T_C$ and $T_{O'O''}$. In the FI state, we find a splitting of the spin waves, an opening of a gap at $\mathbf{q}=(0,0,0.5)$ and a locking of the spin wave energy on the energy values of phonons. In the FM phase, the high energy level magnons vanish while the low energy level ones are still measurable. Note that, in $La_{0.85}Sr_{0.15}MnO_3$, at low tem-

 

perature, a gap in the spin wave spectrum, has also been previously reported.[19]

## II. EXPERIMENT

Single crystals of $La_{1-x}Sr_xMnO_3$ with $x=0.09$ and 0.125, with a volume of about 0.5 $cm^3$ and a 0.6° mosaic spread, were grown by the floating zone method in an image furnace. This technique has been fully described in Ref. 20. The stoichiometry and the single phase quality of the $La_{0.875}Sr_{0.125}MnO_3$ compound, was checked by diffraction measurements, on a powder obtained by grinding a small part of the single crystal. Each sample was mounted on an aluminum block in a double stage helium closed cryogenerator. The temperature regulation is driven by a digital temperature controller and the stability is better than $\pm 0.03$ K in the whole temperature range.

Neutron scattering experiments were performed on triple axis spectrometers installed at either thermal or cold neutron sources at the reactor ORPHEE of the Laboratoire Léon Brillouin. These spectrometers are equipped with vertically focusing monochromators. For elastic and diffuse scattering measurements, flat analyzers were used. We selected an incident neutron beam, with different wave vectors and appropriate filters, following the required $q$ resolution. For inelastic neutron scattering measurements, an horizontally focusing analyzer was chosen in order to increase the signal. At low temperature, positive energy transfer scans were performed at constant scattered neutron wave vector $k_f$ with adapted filter in front of the analyzer. Different final wave vectors ($k_f=2.662$ Å$^{-1}$, $k_f=1.97$ Å$^{-1}$, $k_f\leqslant 1.55$ Å$^{-1}$) were selected according to the energy ranges of the study. All spectra are analyzed by the same method. They are described as the sum of several components, convoluted with the instrumental resolution function $R(\mathbf{Q},\omega)$: a $\delta$ function for the elastic incoherent scattering and Lorentzian laws for the inelastic part. The measured intensity at each point of a scan then reads

$$I(\mathbf{Q_0},\omega_0)=\int R(\mathbf{Q}-\mathbf{Q}_0,\omega-\omega_0)S(\mathbf{Q},\omega)[1+n(\hbar\omega)]d^3Qd\omega$$

with $n(\hbar\omega)$, the Bose statistics and with

$$S(\mathbf{Q},\omega)=C_0\delta(\omega)+\frac{C_1}{(\omega-\omega_1)^2+\Gamma_1(\mathbf{q})^2}+\frac{C_2}{(\omega-\omega_2)^2+\Gamma_2(\mathbf{q})^2}+\cdots.$$

The intensity of the various modes reported in the different following plots, corresponds to their energy integral. Below the Jahn-Teller high temperature transition from a nearly cubic phase, the two studied crystals exhibit, at low temperature, an orthorhombic structure with $Pbnm$ symmetry ($c/\sqrt{2}<a<b$). The orthorhombic unit cell, with only manganese ions, is represented on Fig. 1. The relation between the orthorhombic unit cell parameters and the mean edge of the perovskite cube $a_0=\sqrt[3]{abc/4}$, gives $a\sim a_O\sqrt{2}$, $b\sim a_O\sqrt{2}$, $c\sim 2a_0$. The axes **a** and **b** correspond to the diagonals of the face of the small perovskite cube. Reversely, the direction $[1,1,0]_{\text{ortho}}$ in the orthorhombic notation, corresponds to the edge of the perovskite cube. The **c** axis has the same direction [0,0,1], in both symmetry : cubic or orthorhombic. The orthorhombic parameters at low temperature are for $La_{0.91}Sr_{0.09}MnO_3$, $a=5.53$ Å, $b=5.62$ Å, $c=7.75$ Å and for $La_{0.875}Sr_{0.125}MnO_3$, $a=5.52$ Å, $b=5.54$ Å, $c=7.80$ Å. It appears that the orthorhombicity of the last compound is very small. However, for the sake of a general coherence, we use $\mathbf{Q}=\tau+\mathbf{q}$, with $\tau$ defined in the orthorhombic $Pbnm$ indexation for both compounds. The crystals were aligned with an horizontal scattering plane defined by the orthogonal directions: [110] and [001], parallel to two orthogonal edges of the small perovskite cube. As an effect of the Jahn-Teller structural transition, the crystals are twinned. The consequence for neutron scattering experiments is explained in the Appendix at the end of the paper.

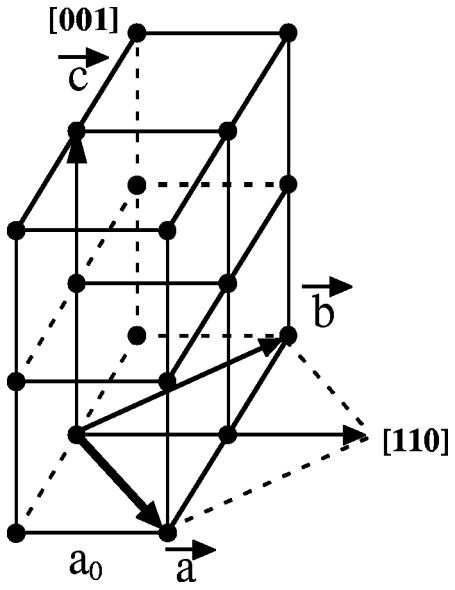


FIG. 1. Scheme of the structure of $La_{1-x}Sr_xMnO_3$ with $x=0.09$ and 0.125. Only Mn ions are represented. The orthorhombic unit cell **a**,**b**,**c**, is shown in relation with the small perovskite cube. $a_0$ is the edge of the cube. Reduced coordinates of a wave vector **Q** $(Q_H,Q_K,Q_L)_{\text{ortho}}=(Q'_H,Q'_K,Q'_L)_{\text{cub}}$ follow the relations $Q'_H=0.5(Q_H-Q_K)$, $Q'_K=0.5(Q_H+Q_K)$, $Q'_L=\frac{1}{2}Q_L$.

## III. $La_{0.91}Sr_{0.09}MnO_3$

$La_{0.91}Sr_{0.09}MnO_3$ is located in the phase diagram just at the limit of the vanishing of the canted antiferromagnetic state (CAF).[21] The study of the intensity of Bragg peaks has allowed the determination of (i) the ferromagnetic transition temperature $T_c=138$ K and (ii) the CAF transition temperature $T_N=120$ K and the value of the canting angle at low temperature: 56°. (90° corresponds to the full ferromagnetic ordering.) The comparison with $La_{0.94}Sr_{0.06}MnO_3$ reveals an evolution of the magnetic features: the occurrence of a ferromagnetic phase between 138 and 120 K and a step increase

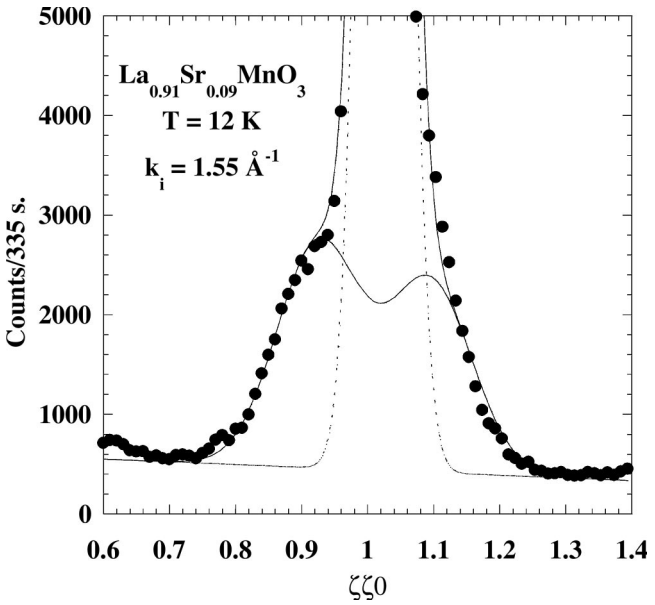


FIG. 2. Diffuse scattering around the (110) Bragg peak of the $x_{Sr}=0.09$ compound. The dotted line fits the Bragg peak and the broken line fits the diffuse scattering (Gaussian functions).

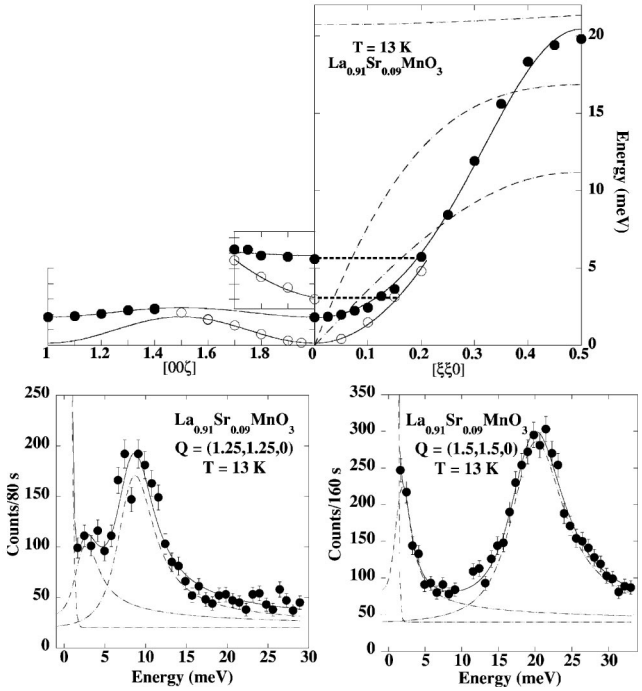


FIG. 3. Higher panel: Dispersion curves of spin waves of the $x_{Sr}=0.09$ compound, propagating along $[0,0,\zeta]$ (left panel) and along $[\xi,\xi,0]$ (right panel). The inset shows the dispersion along $[0,0,\zeta]$ of modes taken at $(0.15,0.15,\zeta)$ (empty symbol), and at $(0.2,0.2,\zeta)$ (full symbol), respectively. Solid lines are the fit of the spin wave dispersion laws, broken lines represent the phonons measured at room temperature and at large **Q** values. Lower panel: Examples of spectra taken, respectively, at $\mathbf{Q}=(1.25,1.25,0)$ and at $\mathbf{Q}=(1.5,1.5,0)$. On each spectrum, the mode measured at small energy belongs to the [001] direction of domain 2 which is superposed on the [1,1,0] direction of domain 1 due to the twinning (see Fig. 12).

of the canting angle (the value is only 13° for $La_{0.94}Sr_{0.06}MnO_3$).

The study of the diffuse scattering around the (110) Bragg peak shows a symmetrical modulation at low temperature (Fig. 2), as already measured in low Sr- or Ca-doped manganites.[11,12] This can be pictured by a liquidlike distribution of ferromagnetic droplets with a net magnetization along the c axis. A rough fit of the diffuse scattering with a Gaussian and a Guinier law gives a characteristic size of about 32 Å and an average distance between the droplets of about 50 Å . This means that this sample is closer to the percolation threshold, at least in the basal plane $(a,b)$, than the sample with $x_{Sr}=0.06$. As this crystal is twinned, the anisotropy of the droplet shape could not be determined as done in the case of an untwinned crystal of $La_{0.94}Sr_{0.06}MnO_3$.[11] We explain these ferromagnetic inhomogeneities by a charge segregation, the ferromagnetic droplets being hole-rich and the remaining AF matrix being hole poor.[11,12] This may remind large magnetic polarons theoretically predicted in similar systems.[7]

Associated with this peculiar modulated ground state, made of two interconnected magnetic media, two spin wave branches with two distinct gaps are measured by inelastic neutron scattering at low temperature: one, in a low-energy range and the second, in a higher-energy domain, as in the previously studied low-doped systems $x_{Ca}=0.05,0.08$, $x_{Sr}=0.06$.[11,13–15] The spin wave dispersion curves are reported on Fig. 3. On the same figure, in the lower panel, two spectra from the high energy branch are shown at special $Q$ values for a future comparison with the compound $La_{0.875}Sr_{0.125}MnO_3$. The high energy branch with a large gap of 1.82 meV is well understood in the frame of a Heisenberg model. Two superexchange integrals are determined: one, ferromagnetic, $J_1=1.15$ meV, coupling first Mn neighbors in the basal plane $(a,b)$, the second one, very much smaller, antiferromagnetic, coupling the AF ions along the $c$ axis $J_2=-0.2$ meV. The low energy branch, with a small gap of 0.14 meV, appears also very anisotropic. It is worth noting that the low energy branch has measurable intensity in the low $q$-value range along [110], only around the F (110) Bragg peak, while, in the same q-range, the high energy one is only measured around the AF (111) Bragg peak. Moreover, it is clearly seen, on Fig. 3, that this low energy branch merges into the high energy curve just beyond $q=(0.2,0.2,0)$. A detailed study of the dispersion of the magnetic modes along $q=[0.15,0.15,\zeta]$ and $q=[0.2,0.2,\zeta]$ has allowed to precise the nature of the dispersion (see the inset of Fig. 3). The first mode, very dispersed along $[00\zeta]$, belongs to the low energy branch, while the weak dispersion, along the same direction, of the second one, is well explained by the value of the AF superexchange coupling $J_2$. Finally, this low-energy branch is well described by the following quadratic dispersion law : $\omega=0.14+D_{xx}[q_x^2+q_y^2]+D_{xz}[q_xq_z+q_yq_z]+D_{zz}q_z^2$, with $D_{xx}=48$ meV Å$^2$; $D_{zz}=25$ meV Å$^2$ and $D_{xz}=16.7$ meV Å$^2$. We recall that in the pure $LaMnO_3$, a single anisotropic spin wave branch is observed, related to anisotropic SE. On doping, in addition to a similar anisotropic spin wave branch as observed in pure

$LaMnO_3$, a second spin wave branch, in a lower energy range, appears. In Ref. 15, a general evolution with the Ca-doping rate, of the characteristic magnetic parameters describing both dispersion branches has been reported. The present new results concerning the compound with $x_{Sr}=0.09$, complete very well the previous works.[11]

The originality of these results is that they emphasize a new step in the ferromagnetic state, in the basal plane (a,b). The comparison of the present findings with those obtained in the compound $La_{0.94}Sr_{0.06}MnO_3$, are summarized as follows. The high-energy magnon branch displays the same gap and determines two exchange integrals varying smoothly, linearly, with the doping rate *x*, as predicted by Feiner and Olés.[22] Concerning the low-energy magnon branch, a drastic change is observed. In the compound $La_{0.94}Sr_{0.06}MnO_3$, its dispersion is isotropic, with an intensity which falls down with increasing *q* vector in the basal plane, which makes measurements very difficult. In $La_{0.91}Sr_{0.09}MnO_3$, this low-energy branch appears very anisotropic (see the above dispersion law). In the basal plane, this ferromagnetic coupling strengthens, suggesting that the system is very near to the percolation threshold. [Interestingly, this peculiar spin wave branch merges into the spin wave branch related to the SE coupling, close to $q=(0.25,0.25,0)$, where a large gap opens in the spin wave spectrum of the compound $La_{0.875}Sr_{0.125}MnO_3$.] By contrast, along the *c* axis, this type of ferromagnetic coupling cannot develop due to the persisting AF order. Similar results have been found recently in the $x_{Ca}=0.10$ compound.[23]

Finally, for a comparison with the study of the $La_{0.875}Sr_{0.125}MnO_3$ compound, described hereafter, where magnon and phonon anomalies are revealed, the acoustic (TA, LA) and the lowest longitudinal optical (LO) phonon branches were measured. Measurements at room temperature are reported on Fig. 3 as broken lines. Here, as in the following, we benefit of the selection rules for neutron scattering, to separate phonon from magnon measurements. The range of the energy values of phonons is similar to that of spin waves. The temperature study of the phonon modes at $\mathbf{Q}=(0,0,4.4)$, for example, does not reveal any anomaly at $T_C$ or at $T_N$; in particular, the phonon energies remain constant with temperature. Finally, at room temperature, an important quasielastic scattering reveals that large magnetic fluctuations persist.

## IV. $La_{0.875}Sr_{0.125}MnO_3$

$La_{0.875}Sr_{0.125}MnO_3$ undergoes two low-temperature phase transitions revealed by magnetization and resistivity measurements. Below the ferromagnetic transition, at $T_C$, the resistivity first decreases (insulator-metal transition) and shows an upturn below $T_{O'O''}$,[17] concomitantly with a step increase of magnetization. The transition temperatures, determined from Bragg peak intensities [(200) for $T_C$, superstructure Bragg peaks $(0,0,2\ell+1)$ and $(0,0,\ell+0.5)$, for $T_{O'O''}$], agree well with those found in the literature, Refs. 16–18: $T_C=181$ K and $T_{O'O''}=159$ K. Below $T_{O'O''}$, the orthorhombicity strongly decreases and the three characteristic Mn-O distances become very close to each other. The precise structure is not yet fully solved. However this structure is known to be triclinic.[24] But, owing to the resolution of neutron spectrometers, the mean structure of this FI phase can be described by the Pbnm symmetry.

### A. Phonons and Spin waves at 14 K

The phonon dipersion curves (TA, LA, LO) have been measured at several temperatures along [001] [Fig. 4(b) diplays the curves at 14 K], and at room temperature and 14 K, along [100] (Fig. 5 right panel diplays the curves at room temperature). The TA, LA, LO branches look similar to those measured in $La_{0.91}Sr_{0.09}MnO_3$ and similar compounds.[25] At room temperature as at low temperature in the FI phase, they reflect the perovskite cubic structure. In particular, along [001], no folding is observed due to the new superstructure Bragg peaks $(0,0,2\ell+1)$ and $(0,0,\ell+0.5)$. However, anticipating the results displayed in the next section, we mention that anomalies occur in TA and LA frequencies, at both transition temperatures, peculiarly at $\mathbf{q}=(000.5)$.

By contrast, the spin waves in $La_{0.875}Sr_{0.125}MnO_3$ exhibit an important change with respect to the spin waves determined in $La_{0.91}Sr_{0.09}MnO_3$. In a FI phase, one should have expected an isotropic ferromagnetic coupling (of DE or SE origin) leading to a single spin wave dispersion law $\hbar\omega(\text{meV})=4JS[1-\cos(2\pi\zeta)]$. Instead of that, at 14 K, a complex spin wave curve, is measured, splitted in the whole *q* range. In spite of this apparent complexity, interesting features appear both in the variation of the energy $\omega(q)$ and in the intensity $I(q)$ at specific *q* values in direct relation with the new superstructure Bragg peaks, characteristic of this FI phase. The spin wave dispersion curves propagating along [001], at $T=14\ K$ are reported in Fig. 4(a), using solid (empty) symbols for main (minor) intensity. The corresponding evolution of the intensity, along [001], is plotted in Fig. 4(c).

We describe now the spin wave dispersion curves from q=0 to the zone boundary of the cubic structure.

(i) In the range $(000)<\mathbf{Q}<(002.225)$, at small $\mathbf{q}$ values, $(000)<\mathbf{q}<(000.225)$, this dispersion curve appears splitted into two curves, when measured with an appropriate resolution. As an example, a spectrum measured at $\mathbf{Q}=(0,0,2.2)$ is shown in Figs. 4(d) and 4(e). An improvement of the fitting process by a factor 3, is obtained when the spectrum is fitted with two modes [Fig. 4(e)] instead of one mode [Fig. 4(d)]. Fitting these small *q* dispersion curves with the $\omega=\omega_0+Dq^2$ law, two distinct gaps $\omega_0$ (0.2 and 0.33 meV) and two distinct isotropic stiffness constants *D* (56 and 69 meV Å $^2$)are determined [see the inset of Fig. 4(a)].

(ii) At $\mathbf{Q}=(002.25)$ and beyond, the splitting becomes much larger and the locking of the spin wave energy on the phonon ones is obvious. Around $\mathbf{Q_0}=(002.5)$, a wide gap opens with a bending of the lower energy spin wave branch. The two energies defining this gap precisely correspond to that of TA phonon for the lower one and to that of LA phonon, for the upper one, with nearly equal intensities [see Fig. 4(c)]. The corresponding spectrum shown in Fig. 6 (lower panel) which exhibits two modes in the 5–15 meV range, can be interestingly compared with the spectrum taken at the

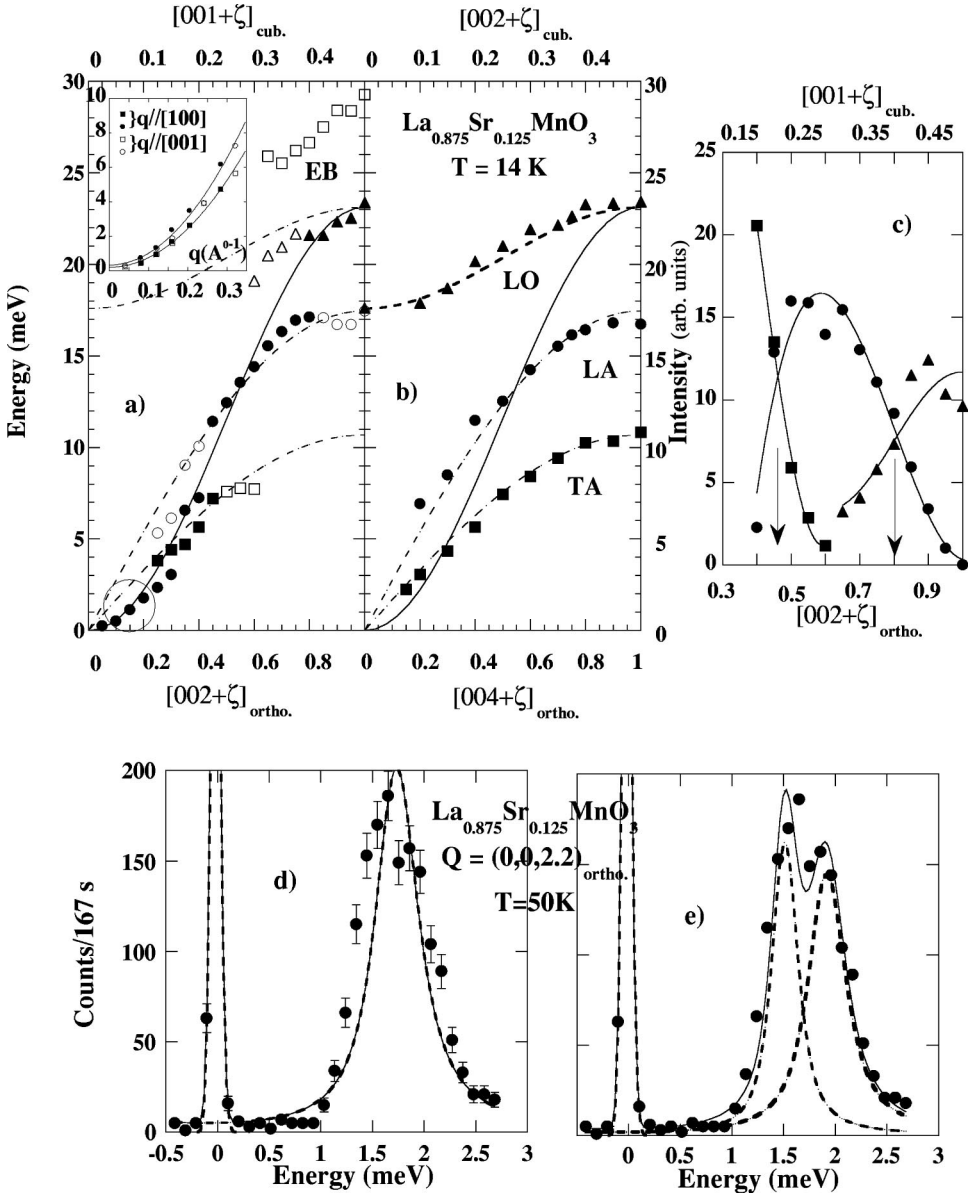


FIG. 4. [001] Direction. (a) Magnetic excitations along (002) $\leqslant \mathbf{Q} \leqslant$ (003). (b)Phonons along (004) $\leqslant \mathbf{Q} \leqslant$ (005). The solid line from 0 to 23 meV represents a ferromagnetic spin wave curve with $J_{\text{eff}}=1.45$ meV (see text). The error bars are smaller than the size of symbols. (■) TA branch was measured along $[22\zeta]$. (●)LA branch, (▲)LO branch. Broken lines represent best fits of phonon curves, The inset displays the splitted magnetic branches. (c) Intensities of the spin wave modes. The symbols are the same as in (a). The arrows indicate the value of **Q** where intensities cross. The lower panel displays (d) a spectrum at $\mathbf{Q}=(0,0,2.2)$ [or $(0,0,1.1)_{\text{cub}}$], fitted with one magnon mode and (e) the same spectrum fitted with two modes.

same $|\mathbf{Q}|$ value, for the $x_{\text{Sr}}=0.09$ compound (Fig. 3, low left panel) where a single mode is observed in the same energy range.

(iii) At and beyond $\mathbf{Q_0}=(002.5)$, the energy of the magnetic modes with main intensity, locks successively on three levels: from the values of the energy of TA phonons, to the values of the energy of LA phonons, and on the values of the energy of the lowest LO phonons. As displayed in Fig. 4(c), the transfer of intensity between these levels occurs around $Q \approx (002.5)$ and $Q \approx (002.75)$. Similarly to $\mathbf{Q_0}=(002.5)$, a small tendency to a bending of the spin waves close to LA, occurs at $Q \approx (002.75)$. Finally, spin wave modes with maximum intensity determine a ferromagnetic spin wave dispersion law $\hbar\omega(\text{meV})=4J_{\text{eff}}S[1-\cos(2\pi\zeta)]$ with an effective first neighbor exchange integral $J_{\text{eff}}=1.45$ meV [see solid line in Fig. 4(a)]. In the range $(002.5) \leqslant \mathbf{Q} \leqslant (003.5)$, around 25-30 meV, we mention additional modes, with a poor intensity. They define what is called an extra branch [EB on Fig. 4(a)]. As they are not detected at larger value of **Q** and disappear upon increasing the temperature towards $T_{O'O''}$, they have a magnetic character, characteristic of the FI phase.[26,27]

To sum up, along [001], the anomalous variations of the energy and intensity of the spin waves, reveal specific $Q$ values, around (002.25), (002.5), (002.75), in direct relation with superstructure Bragg peaks associated with new periodicities, $2a_0$ for the Bragg peak at $(002\ell+1)$, and $4a_0$ for the Bragg peak at $(00\ell+0.5)$. In particular, the bending at (002.5) could reflect a tendency to a folding of the spin wave curve due to the new (003) zone center. By continuity, the abovementioned splitting observed at low $q$, may proceed from the same physics. (In particular, it should not be related to the superposition of two directions because of the twinning.)

(iv) A similar splitted spin wave dispersion curve is observed along [100] (Fig. 5, left panel). At small $q$ values, as along [001], two isotropic dispersion curves are determined [see the inset of Fig. 4(a)]. At $\mathbf{q}=(0.35,0,0)$, which has the

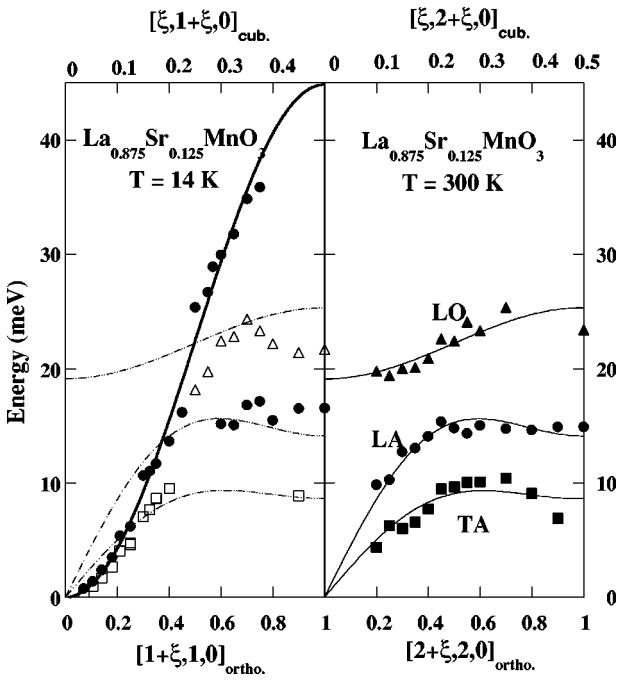


FIG. 5. [100] Direction. Magnetic excitations along (1,1,0) $\leqslant \mathbf{Q} \leqslant$ (2,1,0) at 14 K (left panel) and phonon dispersion curves along (2,2,0) $\leqslant \mathbf{Q} \leqslant$ (3,2,0) at 300 K (right panel). The thick solid line from 0 to 45 meV represents a ferromagnetic spin wave curve with $J_{\text{eff}} = 1.45$ meV. The error bars are smaller than the size of symbols. Broken and thin solid lines represent best fits of phonon curves at room temperature.

same modulus as $\mathbf{q_0} = (0,0,0.5)$, the opening of a gap occurs. A progressive transfer of the intensity is observed from the low energy level to the upper one till the zone boundary. The magnetic modes of maximum intensity also follow a dispersion law with nearly the same $J_{\text{eff}}$ coupling as that determined in the [001] direction. However, we must underline that the splitted energy levels do not correspond to phonon ones as well as they do along [001]. Especially, near the zone boundary, no locking on a phonon value is observed since the next optical phonon branch lies at much higher energy than the energy of the spin waves.[25]

### B. Temperature behavior of spin waves and phonons

The temperature evolution of these excitations and their comparison at different **Q**, and especially at equivalent $\mathbf{q} = \mathbf{Q} - \tau$, are crucial to know their magnetic or phononic nature. Due to the magnetic form factor of Mn ions and the selection rules of the neutron scattering cross section for phonons, magnetic modes are better measured at small **Q** and phonons at larger **Q**. We have studied many points along the [001] direction: $\mathbf{Q} = (0,0,2+\zeta)$ with $\zeta = 0.2, 0.5, 0.75, 1$, $\mathbf{Q} = (0,0,4+\zeta)$ with $\zeta = -0.55, -0.5, -0.45, 0.5$, and along the [100] direction: $\mathbf{Q} = (1.35,1,0)$ and $\mathbf{Q} = (1.6,1,0)$. In this paper, we shall focus on three peculiar **Q** values along [0,0,1] which are superstructure Bragg peaks in the FI phase [(0,0,2.5), (0,0,4.5),(0,0,3)] and on one value along [1,0,0], $\mathbf{Q} = (1.35,1,0)$.

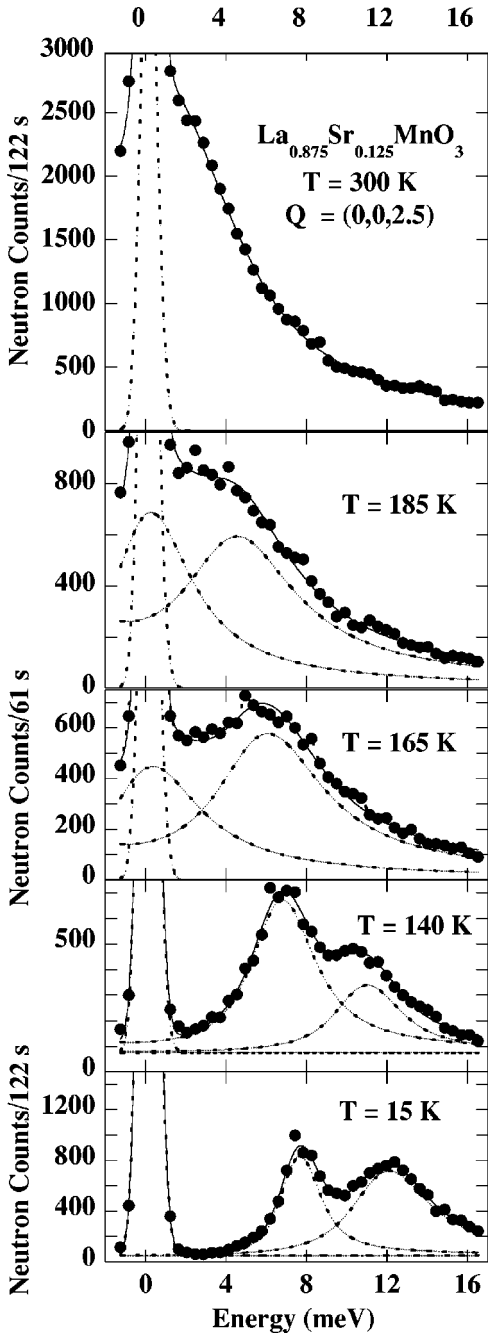


FIG. 6. Temperature evolution of the spectrum measured at $\mathbf{Q} = (002.5)$ [or $(001.25)_{\text{cub}}$], at five temperature values. Dotted lines represent distinct resolution-convoluted modes (see text).

(i) $\mathbf{Q_0} = (002.5)$. The energy-spectra measured at $\mathbf{Q_0} = (002.5)$, and at different temperatures, are reported in Fig. 6. The temperature evolution of the energy and of the intensity of these two modes are reported in Fig. 7 with solid symbols.

As mentioned in Sec. IV, at low temperature, the energy-values of the two modes defining the gap, are the same as those of TA and LA phonon modes. With increasing temperature, the mode located at the LA value has a slightly decreasing energy value, then it vanishes at $T_{O'O''}$. The lower energy mode keeps the TA value up to $T_{O'O''}$ where it starts to

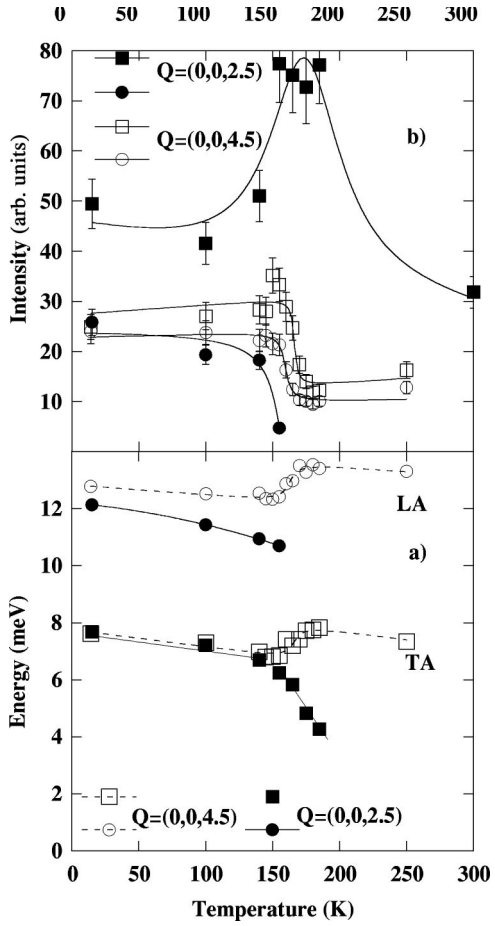


FIG. 7. Temperature evolution (a) of the energy values and (b) of the energy-integrated intensity of the modes measured at $\mathbf{Q}=(002.5)$ [or $(001.25)_{\mathrm{cub}}$], (full symbols) and at $\mathbf{Q}=(004.5)$ [or $(002.25)_{\mathrm{cub}}$] (empty symbols). Broken and solid lines are guides for the eye.

decrease. It softens till $T_C$ where its intensity is maximum. Beyond $T_C$, the softening becomes more abrupt and the mode merges into the quasielastic scattering. At room temperature, quasielastic scattering is still observed, indicating large magnetic fluctuations. As no phonon is measured at this point, at room temperature, we conclude that, despite their energy values close to TA and LA phonon values, both modes are magnetic. However, may a phonon, not measurable at room temperature, appear at $T_C$, dressed as a magnetovibrational (m.v.) mode? A look on the expressions of $(d^2\sigma/d\Omega dE')^{\mathrm{ph}}_{\mathrm{coh}}$ and of $(d^2\sigma/d\Omega dE')_{\mathrm{m.v}}$ in Ref. 28, shows that if we cannot measure a given mode as a pure phonon, we could not measure it as a magnetovibrational mode below $T_C$. But the main argument is given by a recent experiment. We could check the nature of these excitations in an experiment under a magnetic field applied along the **c** axis, parallel to $\mathbf{Q_0}$. Considering the magnetic geometrical factor of the magnetic inelastic neutron scattering cross section,[28] the increase of the intensity at $\mathbf{Q_0}$, under the magnetic field, reveals the mainly transverse character of the spin excitations. In particular, it rules out a possible interpretation in terms of magnetovibrational modes with a longitudinal character.[28] This will be published elsewhere.

(ii) $\mathbf{Q}=(004.5)$. A similar temperature study has been achieved at $\mathbf{Q}=(004.5)$. As this $Q$ value is larger than $\mathbf{Q_0}=(002.5)$, we can think that, at this point, we are measuring rather phonons than magnons. Figure 7 summarizes the values of the energy and of the intensity of the modes (empty symbols), versus temperature, and displays an interesting comparison with the behavior of the modes measured at $\mathbf{Q_0}=(002.5)$ (full symbols). Figure 7(a) shows a slight hardening of the energy of the TA and LA phonon modes, with decreasing temperature from room temperature, as usual. From $T_C$ down to $T_{O'O''}$, in the intermediate FM phase, significant softenings are measured on both phonon modes, of $\sim$12% for TA and of $\sim$8% for LA. Then, a little hardening is again observed down to low temperatures where, finally, the energies of the phonons are the same as those of the magnons. A signature of both transitions is also seen on their intensities [Fig. 7(b)]. Upon decreasing temperature from room temperature value, the intensity of the two modes remains rather constant, then it starts to increase at $T_C$ and shows an abrupt increase with a kind of inflexion point around $T_{O'O''}$, before its saturation, at low temperature, at a value greater than the value measured at room temperature. This variation can be explained by the superposition of a magnetic contribution below $T_C$, since the square magnetic form factor of $Mn^{3+}$ is only 2.5 times smaller at (004.5) than at (002.5).

The softening of the LA and TA modes, in the intermediate FM phase, while concomitantly the magnetic mode measured at $\mathbf{Q}=(002.5)$ hardens, suggests a peculiar magnon-phonon coupling. The coincidence of the value of the TA and LA energies with that of the magnetic modes at $\mathbf{Q}=(0,0,2.5)$, in the FI phase, is hardly believed to be casual. However, we must underline that, contrary to the usual magnon-phonon coupling,[29] in the present case, the damping of magnons and phonons remains small. For the LA and TA phonon modes, the damping constant $\Gamma$ varies from $\sim$2.4 meV at room temperature, to $\sim$1.6 meV at low temperature. Polarized neutron experiments are planned to elucidate this important question.

(iii) $\mathbf{Q}=(003)$. This point, which is also a superstructure Bragg peak, plays essentially the role of the zone boundary for the magnetic excitations. The temperature evolution of the spectrum measured at $\mathbf{Q}=(003)$ is shown on Fig. 8. The energy values and the intensities of the modes are reported on Fig. 9. The signature of both transitions is essentially visible by an abrupt change in the intensity of the modes and not in their energy values which are nearly temperature independent. On Fig. 8(a), the spectrum at 14 K consists of three modes centered successively on the energy values of the LA, LO phonons and on a higher energy-value associated with the extra branch EB [see Fig. 4(a)]. The maximum of intensity is on the LO value. At $T_{O'O''}$, [Fig. 8(c)], the EB mode vanishes whereas a small intensity appears on the TA value. The intensity now is distributed on three energy-values corresponding to TA, LA, LO phonon energy values, with the main part centered on the LA value. From $T_{O'O''}$ to $T_C$, the magnetic intensity on the LO energy value decreases and is progressively transferred to the LA level, while the mode locked on the TA value remains visible in the whole FM phase. At $T_C$, both modes at TA and LO values vanish,

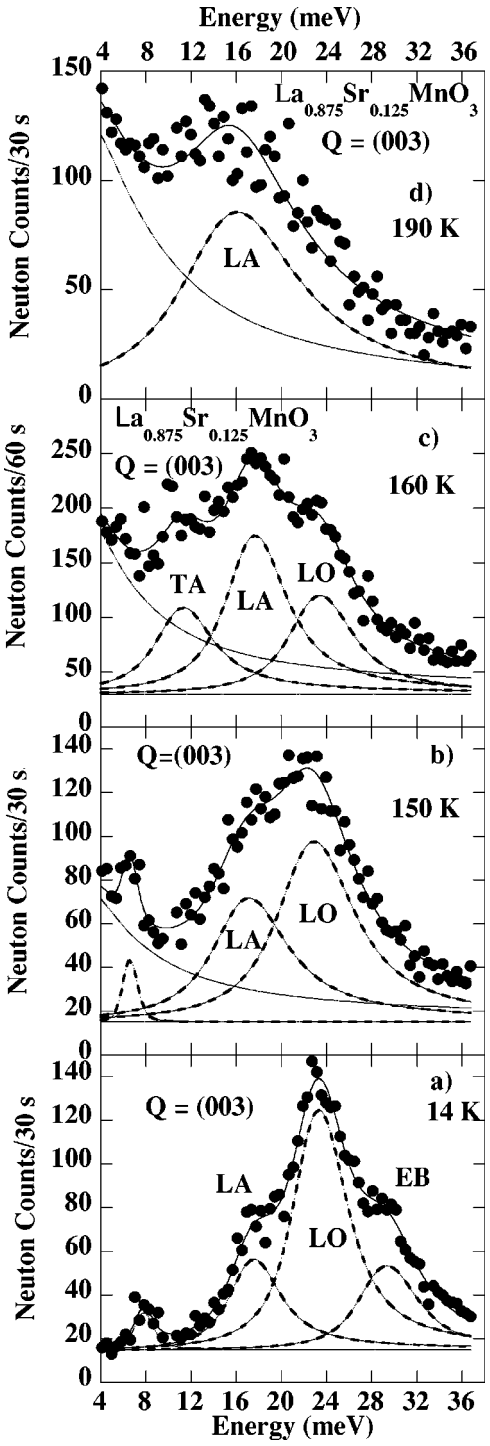


FIG. 8. Temperature evolution of the spectrum measured at $\mathbf{Q}=(003)$ (or $(001.5)_{cub}$), at four temperature values. **(a)**T=14 K, **(b)** T=150 K, **(c)** T=160 K, **(d)** T=190 K. Broken lines represent distinct resolution-convoluted modes (see text). [The small peak at 8 meV in **(a)** and **(b)** is a spurious effect due to the (003) Bragg peak.]

while the intensity of the mode at LA value, reaches its maximum. Finally, at 190 K [Fig. 8(d)] as at 300 K, the energy spectra, very similar, consist of two modes, a quasielastic one, magnetic, and a collective one, which corresponds to the pure LA phonon, with a rather small intensity.

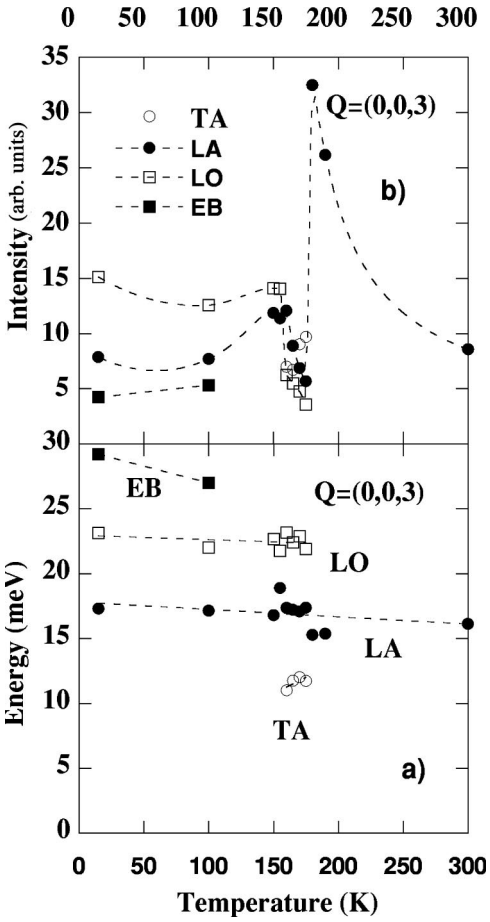


FIG. 9. Temperature evolution of the modes determined at $\mathbf{Q}=(003)$ [or $(001.5)_{cub}$]. **(a)** Energy values. **(b)** Intensity values; note the jump of intensities of LA at $T_C$ and of LO at $T_{O'O''}$. Dotted lines are guides for the eye. (TA, LA, LO mean magnetic modes close to TA, LA, LO phonon energy values, respectively.)

Since at 14 K the same intensity is measured for this mode, one concludes that, also at low temperature in the FI phase, it is a pure LA phonon.

In conclusion, at $\mathbf{Q}=(003)$, the main results are the LA phonon mode is the alone mode measurable at any temperature. In the FM phase, a spin wave mode is superposed at the same energy value, it vanishes in the FI phase. At 15 K, the spin wave mode is essentially located at LO phonon value and, to a lesser extent, on the EB branch. Again, in the intermediate FM phase, only the modes of lower energy mainly remain. As at $\mathbf{Q}=(002.5)$, the transition at $T_{O'O''}$ from FI to FM phase, can be seen by a step variation of the intensity from the highest energy levels to lower energy levels.

(iv) $\mathbf{Q}=(1.35,1,0)$. A same temperature study is performed in the [100] direction (face diagonal of the small perovskite cube), especially at $\mathbf{q}=(0.35,0,0)$. The spectra are reported on Fig. 10. They show the same features as the spectra taken along the [001] direction at (002.5). The temperature behavior of the corresponding energies and intensities are reported on Figs. 11(a) and 11(b). At very low temperature, the inelastic part consists of two modes. Unlike the case of the [001] direction, the values of the energy of both

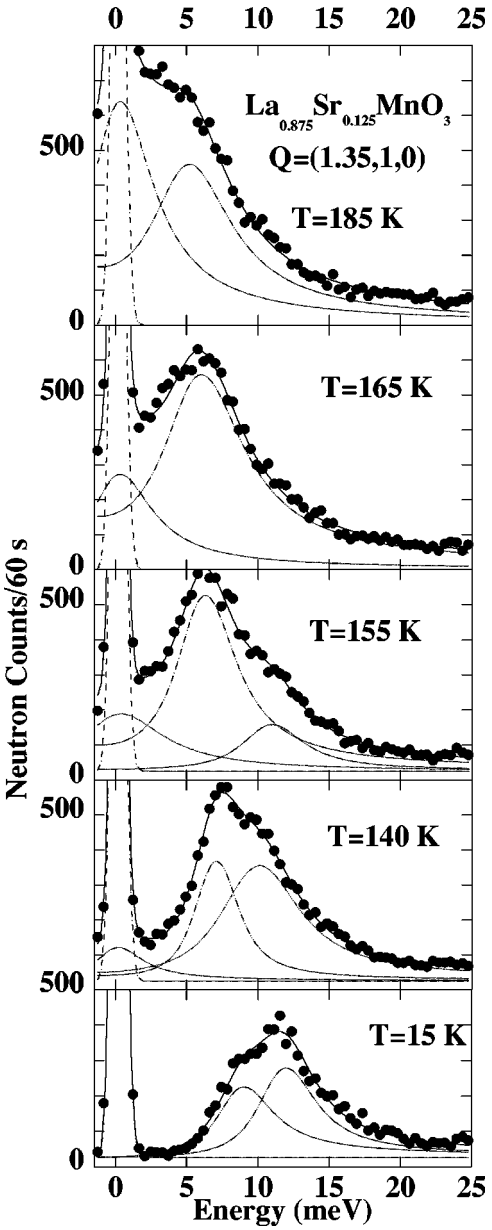


FIG. 10. Temperature evolution of spectrum measured at $\mathbf{Q}=(1.35,1,0)$ [or $(0.175,1.175,0)_{cub}$]. Broken lines represent distinct resolution-convoluted modes (see text).

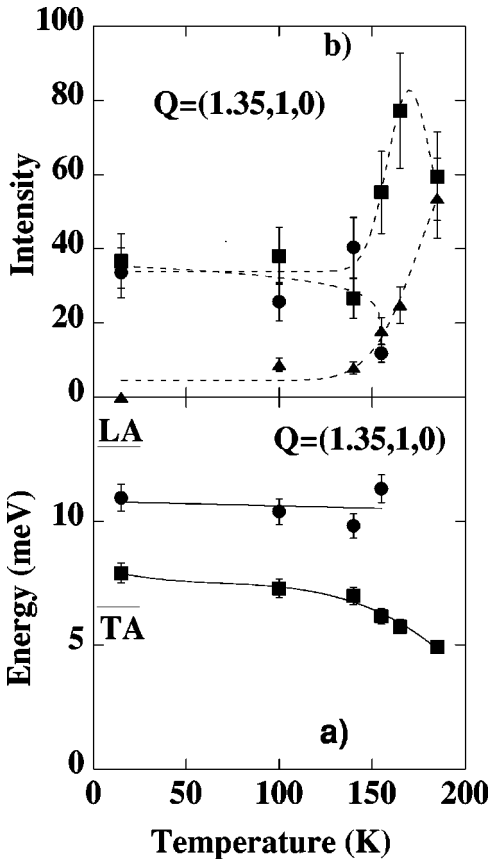


FIG. 11. Temperature evolution of the modes determined at $\mathbf{Q}=(1.35,1,0)$ [(or $(0.175,1.175,0)_{cub}$)]. (a) Energy values. Note that they do not coincide with LA and TA phonon values at low temperature (small thin lines), as well as along [001]. (b) Intensity values; note that, in the $T_{O'O''}<T<T_C$ range, the intensity of the low energy mode (■) increases while that of the high energy mode (●) vanishes. ▲ represents quasielastic intensity. Dotted and solid lines are guides for the eye.

modes do not exactly coincide with the values of the energy of TA and LA phonons [Fig. 11(a)]. As observed along [001], with increasing temperature, the upper mode keeps an almost constant energy value and vanishes at $T_{O'O''}$. The lowest energy mode renormalizes and, above $T_{O'O''}$, in the FM phase, is only observed together with a growing quasielastic scattering. Then it disappears at $T_C$.

To summarize the overall results, three essential features can be underlined. (i) In the FI phase, the spin wave spectrum is splitted in the whole $q$ range. The magnon energies lock on the TA, LA, LO phonon energy values, especially along the [001] direction. (ii) In the FM phase, at any $q$ value, only the lowest energy modes keep magnetic intensity. (iii) Anomalies are measured in the acoustic phonon modes at the superlattice point (000.5), at $T_{O'O''}$ and at $T_C$. More precisely, the transition at $T_{O'O''}$ appears driven by the hardening of the magnon and the softening of the TA phonon energies at (000.5), and occurs just when both energies are equal. Similar anomalies of the spin wave spectrum and the same locking of the magnon at (000.5), on TA phonon energy, are also found in the FI state of Ca-doped manganites, with $x_{Ca}=0.20$.[15,30]

### C. Discussion

At the doping rate $x_{Sr}=0.09$, the new result concerns the low energy spin wave branch, observable here, in a wide $q$ range with an anisotropic dispersion. Although two spin wave branches are expected in a canted antiferromagnetic (CAF) state, their characteristics as well as the $q$ modulation observed in the diffuse scattering, still agree with the picture of an inhomogeneous state: a mean AF, hole-poor state, coexisting with a liquidlike order of hole-rich ferromagnetic clusters, as in the other low-doped compounds.[11,12] At $x_{Sr}=0.125$, which corresponds to the occurrence of a F state, the anomalous spin wave spectrum may indicate also a nonuniform charge distribution. As we measure two spin wave

stiffness constants, at small $q$ values, i.e., on a wide scale in the direct space, we can imagine that this FI phase is made of two interconnected Mn ion subsystems, with different spin and charge, likely associated with some new charge and orbital ordering.[18,31] A charge segregation has been also proposed in this F state by Moreo *et al.*[8] Since at and beyond $q=(0,0,0.5)$, the splitted energy values are close to those of the phonons, it can be speculated that this FI phase is also stabilized by an elastic strain field resulting from a spin-lattice coupling, although different from the classical magnon-phonon coupling.[29] A different explanation has been suggested recently,[32] considering the effect of randomness induced by *A*-site substitution, in the CMR FM phase of manganites.In this model, strong anomalies were found in the spin wave spectrum with the opening of a gap, at a peculiar $q$ value, which scales with the Fermi wave vector. This feature is associated with an inhomogeneous charge distribution induced by the impurities. To apply this theory in the present case, we should speculate that a Fermi level could be defined, and, at least on some short range, one of the two magnetic subsystems should have metallic properties. As suggested in Ref. 32, the $q$ anomaly should vary with the doping. Experiments on the $x=0.15$ compound,[19] show that the gap anomaly persists at the same $\mathbf{q_0}$, it demonstrates that the model does not apply to a FI state. Finally, recent NMR measurements, performed on Ca-doped manganites, have indicated that, even in the FI low-temperature phase, metallic regions exist,[33] which could support some charge segregation picture. Concerning the FM intermediate phase, the main question is why, in this phase, only the lowest energy part of the splitted spin wave branch remains measurable? We can invoke the role of an orbital disorder, as used by Khaliullin and Kilian[5] to explain the renormalization of the magnons observed close to the zone boundary, in the CMR FM phase of manganites with low $T_C$[2]. In the present case, between $T_C$ and $T_{O'O''}$, in the FM phase, the orbital order induced by the Jahn-Teller effect is seriously damaged. It might evolve to a new one below $T_{O'O''}$.[31] During this evolution, large orbital fluctuations could explain the softening of the magnetic coupling. This scheme could also help to understand why, at low temperature, in the FI phase, large magnetic couplings are sharply restored. It could be the effect of the above-quoted new orbital order. However, a difficulty remains. As soon as an orbital order exists, the magnetic coupling must be theoretically anisotropic.[6] In the present case, the spin wave dipersion curves are isotropic. This could be perhaps explained by persisting orbital fluctuations. The spin wave isotropy could be also solved by a peculiar lattice-spin coupling involving isotropic acoustic and low energy optic phonons, not considered by theory until now.

The exact nature of the ground state of the FI phase of $La_{0.875}Sr_{0.125}MnO_3$ is still an open question, but its amazing and complex magnetic excitations, revealed by inelastic neutron scattering, specially at $q$ values related to new lattice periodicities, will have to be taken into account in its future solution.

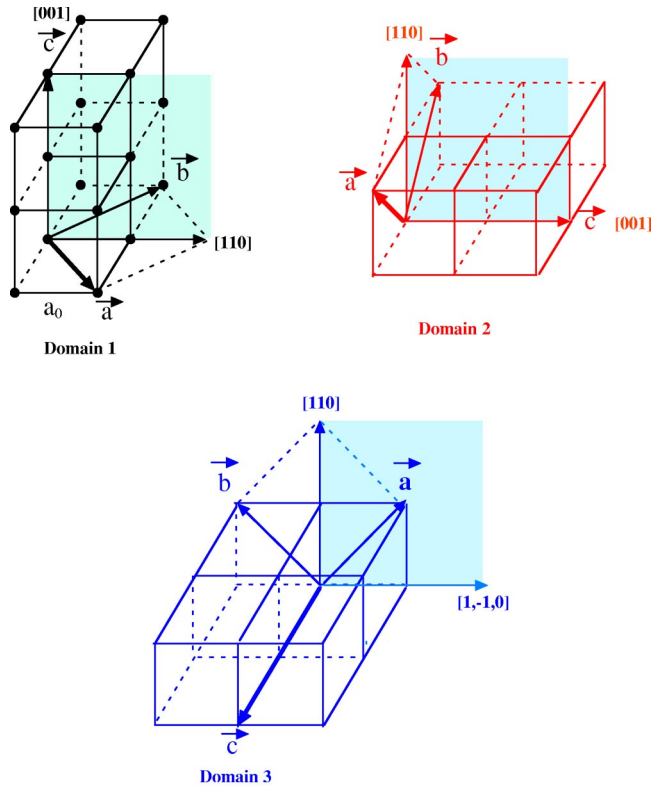


FIG. 12. Representation of the three domains resulting from the high temperature structural transition from a cubic to an orthorhombic symmetry. The **c** axis can be successively along the three edges of the perovskite cube. The shaded square represents the scattering plane of the experiment. Domains 1 and 2 lead to an exchange between the [001] and [110] directions. The scattering plane countains also the basal $(a,b)$ plane of domain 3.


## ACKNOWLEDGMENTS

It is a pleasure to thank G. Khaliullin, D. Khomskii, K. I. Kugel, and A. M. Olès for enlightening discussions.


## APPENDIX

Twinning in perovskites is a very common phenomenon. The occurence of a domain structure in perovskites is due to the fact that at high temperature, the aristotype cubic $Pm3m$ structure is the most stable. On cooling, a structural transition may occur, leading to a lower symmetry. It generates domains related by operators lost during the transition. In perovskites of $Pbnm$ structure, (cell $a_0\sqrt{2}\times a_0\sqrt{2}\times 2a_0$), up to six orientational domains can exist. In our experiment three domains have been found. They are represented in Fig. 12. Each of them corresponds to the alignment of the $Pbnm$ **c** axis along one edge of the perovkite cube. So along the [110] direction of domain 1, the [001] direction of domain 2 and the [110] direction of domain 3 are also observed. Only the direct space is represented here, but as the vectors of the unit $Pbnm$ cell, **a**, **b**, **c**, are, respectively, parallel to the vectors of the reciprocal cell, **a***, **b***, **c***, the superposition of the same directions in the reciprocal space is observed.

Scanning, for instance, along the [001] direction of domain 1, it is possible to measure the Bragg peak (002) and the Bragg peaks (110) of domain 2 and domain 3. If the $q$ resolution of the spectrometer is better than the difference between $|\tau_{002}|$ and $|\tau_{110}|$, these two peaks will be discriminate. It is the case for $La_{0.91}Sr_{0.09}MnO_3$, it is not the case for $La_{0.875}Sr_{0.125}MnO_3$ where the orthorhombicity is too small. The presence of the domain 3 gives us the opportunity to measure also the spin waves and the phonons propagating along the **a** axis direction (Fig. 5).


[1] J. A. Fernandez-Baca, P. Dai, H. Y. Hwang, C. Kloc, and S. W. Cheong, Phys. Rev. Lett. **80**, 4012 (1998).

[2] P. Dai, H. Y. Hwang, Jiandi Zhang, J. A. Fernandez-Baca, S. W. Cheong, C. Kloc, Y. Tomioka, and Y. Tokura, Phys. Rev. B **61**, 9553 (2000).

[3] C. Zener, Phys. Rev. **82**, 403 (1951).

[4] N. Furukawa J. Phys. Soc. Jpn. **65**, 1174 (1996).

[5] G. Khaliullin and R. Kilian, Phys. Rev. B **61**, 3494 (2000).

[6] A. M. Olés and L. F. Feiner, Phys. Rev. B **65**, 052414 (2002).

[7] E. L. Nagaev, Phys. Status Solidi B **186**, 9 (1994); Phys. Rev. B **60**, 455 (1999).

[8] A. Moreo, S. Yunoki, and E. Dagotto, Science **283**, 2034 (1999).

[9] D. Arovas and F. Guinea, Phys. Rev. B **58**, 9150 (1998).

[10] M. Y. Kagan, D. Khomskii, and M. Mostovoy, Eur. Phys. J. B **12**, 217 (1999); M. Y. Kagan and K. I. Kugel, Usp. Fiz. Nauk **171**, 577 (2001) [Phys. Usp. **44**, 553 (2001)].

[11] M. Hennion, F. Moussa, G. Biotteau, J. Rodríguez-Carvajal, L. Pinsard, and A. Revcolevschi, Phys. Rev. B **61**, 9513 (2000).

[12] M. Hennion, F. Moussa, J. Rodríguez-Carvajal, L. Pinsard, and A. Revcolevschi, Phys. Rev. Lett. **81**, 1957 (1998).

[13] M. Hennion, F. Moussa, J. Rodríguez-Carvajal, L. Pinsard, and A. Revcolevschi, Phys. Rev. B **56**, R497 (1997).

[14] F. Moussa, M. Hennion, G. Biotteau, J. Rodríguez-Carvajal, L. Pinsard, and A. Revcolevschi, Phys. Rev. B **60**, 12 299 (1999).

[15] G. Biotteau, M. Hennion, F. Moussa, J. Rodríguez-Carvajal, L. Pinsard, A. Revcolevschi, Y. M. Mukovskii, and D. Shulyatev, Phys. Rev. B **64**, 104421 (2001).

[16] Y. Yamada, O. Hino, S. Nohdo, R. Kanao, T. Inami, and S. Katano, Phys. Rev. Lett. **77**, 904 (1996).

[17] L. Pinsard, J. Rodríguez-Carvajal, A.H. Moudden, A. Anane, A. Revcolevschi, and C. Dupas, Physica B **234-236**, 856 (1997).

[18] Y. Endoh, K. Hirota, S. Ishihara, S. Okamoto, Y. Murakami, A. Nishizawa, T. Fukuda, H. Kimura, H. Nojiri, K. Kaneko, and S. Maekawa, Phys. Rev. Lett. **82**, 4328 (1999).

[19] L. Vasiliu-Doloc, J. W. Lynn, A. H. Moudden, A. M. de Leon-Guevara, and A. Revcolevschi, Phys. Rev. B **58**, 14 913 (1998).

[20] F. Moussa, M. Hennion, J. Rodríguez-Carvajal, H. Moudden, L. Pinsard, and A. Revcolevschi, Phys. Rev. B **54**, 15 149 (1996).

[21] G. L. Liu, J. S. Zhou, and J. B. Goodenough, Phys. Rev. B **64**, 144414 (2001).

[22] L. F. Feiner and A. M. Olés, Physica B **259-261**, 796 (1999).

[23] P. Kober (unpublished).

[24] M.T. Fernandez-Diaz and J. Rodríguez-Carvajal, (unpublished).

[25] W. Reichardt and M. Braden, Physica B **263-264**, 416 (1999).

[26] P. Reutler, F. Moussa, M. Hennion, and F. Wang, J. Magn. Magn. Mater. **242-245**, 689 (2002)

[27] F. Moussa, M. Hennion, P. Kober, F. Wang, J. Rodríguez-Carvajal, P. Reutler, Y. M. Mukovskii, and D. Shulyatev, J. Magn. Magn. Mater. **258-259**, 259 (2003).

[28] S. W. Lovesey, *Theory of Neutron Scattering from Condensed Matter* (Clarendon Press, Oxford, 1987), Vol. 1, p. 122, Vol. 2, pp. 1, 35, 63.

[29] N. Furukawa, J. Phys. Soc. Jpn. **68**, 2522 (1999).

[30] M. Hennion, F. Moussa, F. Wang, J. Rodríguez-Carvajal, Y. M. Mukovskii, and D. Shulyatev, cond-mat/0112159 (unpublished).

[31] H. Nojiri, K. Kaneko, M. Motokawa, K. Hirota, Y. Endoh, and K. Takahashi, Phys. Rev. B **60**, 4142 (1999).

[32] Y. Motome and N. Furukawa, cond-mat/0203041 (unpublished).

[33] G. Papavassiliou, M. Fardis, M. Belesi, T. G. Maris, G. Kallias, M. Pissas, D. Niarchos, C. Dimitropoulos, and J. Dolinsek, Phys. Rev. Lett. **84**, 761 (2000).